

# Development of Ni-Al<sub>2</sub>O<sub>3</sub> *In-Situ* Nanocomposite by Reactive Milling and Spark Plasma Sintering

V. UDHAYABANU, K.R. RAVI, K. MURUGAN, D. SIVAPRAHASAM,  
and B.S. MURTY

In the present study, Ni-30 vol pct Al<sub>2</sub>O<sub>3</sub> *in-situ* nanocomposite was developed by reactive milling of NiO-Al-Ni powder mixture followed by spark plasma sintering (SPS). During milling, fcc to hcp transformation was observed in Ni(Al) phase and it transformed back to fcc phase around 773 K (500 °C). The hardness and yield strength of Ni-30 vol pct Al<sub>2</sub>O<sub>3</sub> nanocomposite are approximately two times higher than that of pure Ni of similar grain size. The improved mechanical properties of nanocomposite are attributed to the presence of alumina particles of nanometer size.

DOI: 10.1007/s11661-011-0602-6

© The Minerals, Metals & Materials Society and ASM International 2011

## I. INTRODUCTION

NANOCOMPOSITES, in which both the matrix and the reinforcement are nanocrystalline or the nanoreinforcement in microcrystalline matrix, exhibit superior mechanical properties compared to their microcrystalline counterpart with similar volume fraction of reinforcement particles. *In-situ* formation of the reinforcement particles by powder metallurgy route is reported to overcome the difficulty in dispersion and segregation problems of very fine reinforcement particles normally being faced in casting route. Moreover, the *in-situ* reinforcement particles are thermodynamically stable and compatible with the matrix.<sup>[1]</sup> Mechanical alloying is a popular technique to synthesize nanocrystalline, amorphous and intermetallics. In addition, development of nanocomposites by activating the displacement reaction where the metal oxides are reduced by more reactive metal to a pure metal is also one of the applications of the mechanical alloying.<sup>[2,3]</sup>

Nickel was widely used as coating material since it is strong, tough, and resistant to corrosion, erosion, and abrasion. However, during severe environmental and stress conditions, the mechanical properties deteriorate. Hence, one of the methods to improve this is reinforcing Ni with hard particles such as Al<sub>2</sub>O<sub>3</sub>,<sup>[4-7]</sup> CeO<sub>2</sub>,<sup>[8]</sup> TiO<sub>2</sub>,<sup>[9-11]</sup> ZrO<sub>2</sub>,<sup>[12-14]</sup> SiC,<sup>[15-17]</sup> WC,<sup>[18-20]</sup> and

TiC.<sup>[21,22]</sup> These particles act as barriers to dislocation motion within the metal matrix and increase the strength by Orowan hardening phenomena. Moreover, additional benefit can be realized if the particles pin the grain boundaries, thereby impeding grain growth during heat treatment.<sup>[23]</sup> All these preceding reinforcing particles were added externally to Ni matrix. In the present work, an attempt has been made to develop *in-situ* nano-Al<sub>2</sub>O<sub>3</sub> particles reinforced in Ni matrix (Ni-30 vol pct Al<sub>2</sub>O<sub>3</sub>), by subjecting the NiO-Al-Ni powder mixture to reactive milling. The phase evolution during milling and subsequent heating was analyzed. The microstructure and mechanical properties were investigated after the spark plasma sintering (SPS) and compared with the monolithic Ni.

## II. EXPERIMENTAL DETAILS

Reactive milling was carried out in a planetary ball mill (Pulverisette-5, Fritsch, GmbH, Idar oberstein, Germany) for NiO-8 wt pct Al-59 wt pct Ni powder mixture in order to obtain Ni-30 vol pct Al<sub>2</sub>O<sub>3</sub> nanocomposite powder. Milling was carried out at the ball to powder ratio of 10:1 using tungsten carbide vials and tungsten carbide balls of 10-mm diameter. Toluene was used as a process controlling agent to avoid oxidation and excessive cold welding of powders to vials and balls. The milling speed was maintained as 300 rpm. Phase and structural evolution during milling and heating was analyzed using X-ray diffractometry (Bruker AXS Inc., Madison, WI), with Cu K<sub>α</sub> radiation. Crystallite size measurement was made using Voigt X-ray peak profile analysis after eliminating the strain and instrumental broadening contributions.<sup>[24]</sup> Differential scanning calorimetry (DSC) was carried out for the 20-hour milled powder at the heating rate of 20 °C/min in argon atmosphere using a Netzsch STA 409 PC (Netzsch, GmbH, Selb/Bavaria, Germany). Chemical analysis for tungsten was carried out using Optima 5300 DV (Perkin

---

V. UDHAYABANU, Assistant Professor, is with the Department of Metallurgical Engineering, PSG College of Technology, Coimbatore 641 004, India, and is also with the Department of Metallurgical and Materials Engineering, Indian Institute of Technology Madras, Chennai 600 036, India. K.R. RAVI, Assistant Professor, is with the PSG, Institute of Advanced Studies, Coimbatore 641 004, India, and is also with the Department of Metallurgical and Materials Engineering, Indian Institute of Technology Madras. K. MURUGAN and D. SIVAPRAHASAM, Scientists 'C', are with the International Advanced Research Centre for Powder Metallurgy and New Materials (ARCI), Hyderabad 500 005, India. B.S. MURTY, Professor, is with the Department of Metallurgical and Materials Engineering, Indian Institute of Technology Madras. Contact e-mail: murty@iitm.ac.in

Manuscript submitted June 22, 2010.

Article published online January 27, 2011

elmer, Shelton, CT) inductively coupled plasma–optical emission spectroscopy (ICP-OES) in order to determine the tungsten carbide contamination in the 20-hour milled powder. The as-milled powders were consolidated to  $5 \times 15$  mm pellets in a graphite die and consolidated under a uniaxial pressure of 75 MPa, using a SPS-1050 apparatus (Sumitomo Coal Mining, Kangawa, Japan) at 1273 K (1000 °C) for 5 minutes in a vacuum of  $<10^{-3}$  Pa. For comparison, pure Ni was also milled for 20 hours and consolidated at slightly lower temperature of 973 K and 1073 K (700 °C and 800 °C).

Microstructural analysis was carried out for bulk consolidated samples using a PHILIPS\* CM20 trans-

\*PHILIPS is a trademark of FEI Company, Hillsboro, OR.

mission electron microscope (TEM) operating at 200 kV. For the TEM analysis, the samples were prepared by Ar-ion milling preceded by dimpling. Density of bulk samples was measured by the Archimedes method. The hardness of the compacts was measured using a microhardness tester under a load of 300 g for 15 seconds. The average of 20 indentations was considered as the Vickers microhardness value. The compression test was carried out on a  $2.5 \times 3$  mm cylindrical sample at the strain rate of  $10^{-4} \text{ s}^{-1}$ .

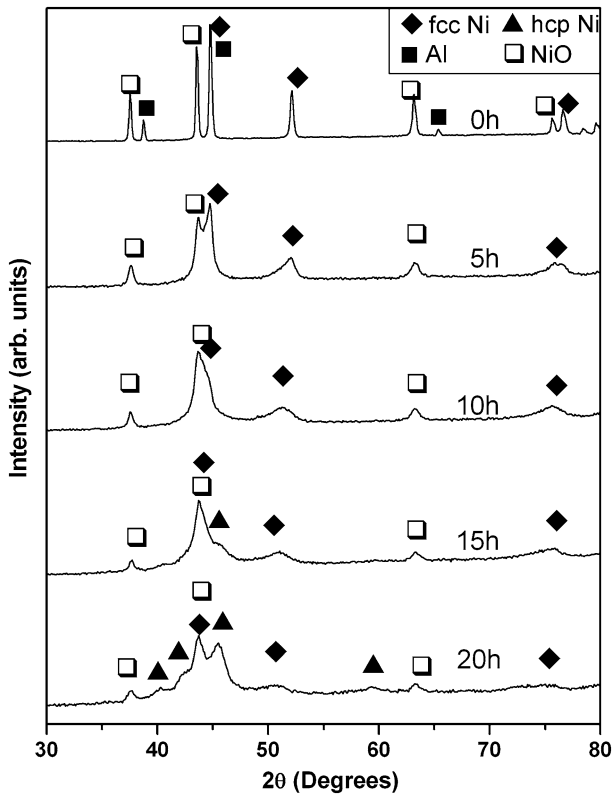


Fig. 1—XRD patterns of NiO, Al, and Ni powder mixture corresponding to Ni-30 vol pct  $\text{Al}_2\text{O}_3$  composition as a function of milling time.

### III. RESULTS

#### A. Phase Formation during Milling and Heating

Figure 1 shows the X-ray diffraction (XRD) patterns of unmilled and milled NiO-Al-Ni powder mixture corresponding to Ni-30 vol pct  $\text{Al}_2\text{O}_3$  nanocomposite. During reactive milling, the observations made after 5 hours of milling are the shift and the broadening of the Ni peaks and the decrease in the NiO peak intensity. The decrease in the NiO peak intensity and the disappearance of Al peak indicate the start of NiO reduction in 5-hour milling. The shift in the Ni peak toward the lower angle side indicates that the Ni formed solid solution with the Al available for the NiO reduction. The extent of NiO reduction was calculated approximately from the change in the integrated intensity of NiO (111) peak with respect to milling time using the formula mentioned elsewhere.<sup>[25]</sup> After 5 hours of milling, the extent of NiO reduction is calculated to be 50 pct and the remaining Al available for Ni(Al) formation in 5-hour milling is  $\sim 5$  wt pct (Figure 2). The position of Ni(Al) peaks continuously shifted to

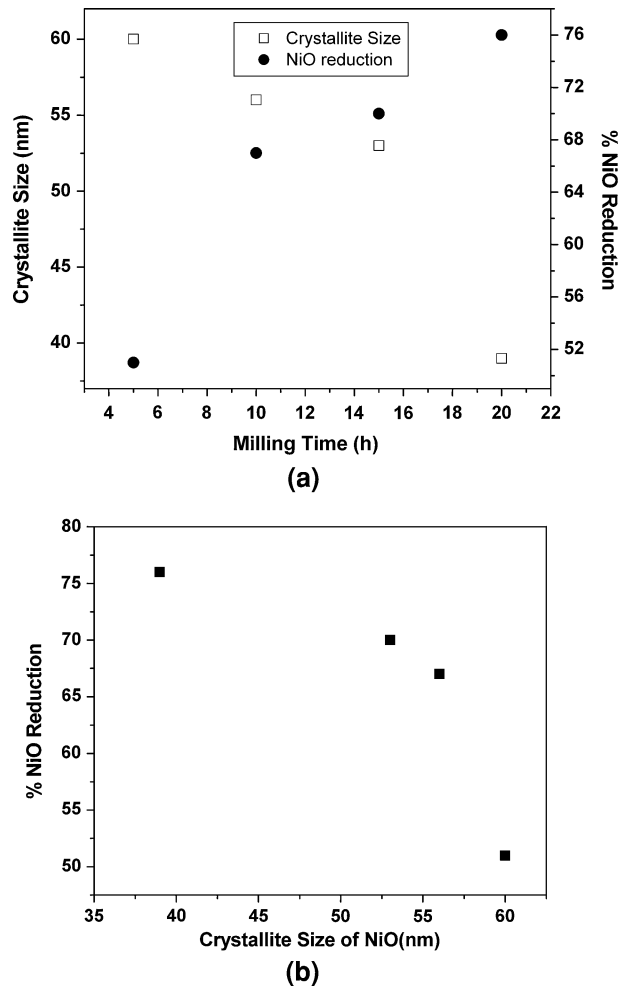


Fig. 2—(a) Crystallite size and NiO-Al-Ni powder mixture corresponding to Ni-30 vol pct  $\text{Al}_2\text{O}_3$  composition with respect to milling time and (b) percentage reduction of NiO with respect to crystallite size of NiO.

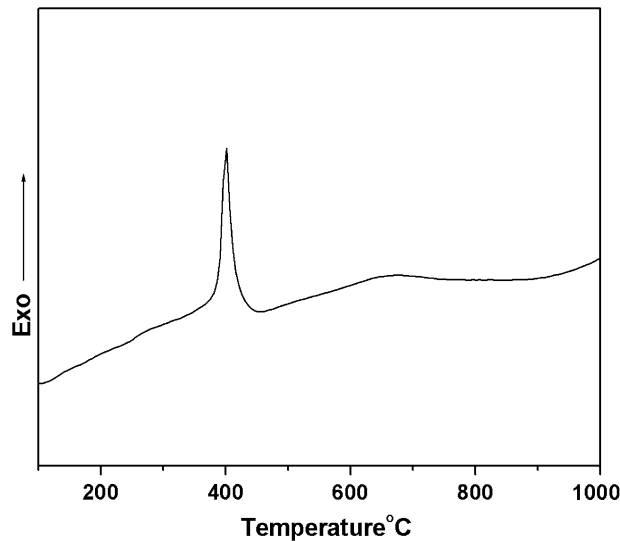


Fig. 3—DSC traces of 20 h milled NiO-Al-Ni powder mixture corresponding to Ni-30 vol pct  $\text{Al}_2\text{O}_3$  composition.

lower angles accompanied by gradual broadening with milling time, indicating a continuous increase in unit cell volume with refinement of crystallite size. After 15 hours of milling, a new peak, which partially overlaps with the NiO(200)/Ni(Al)(111) peak, appeared and it has been identified as the most intense peak (101) of hcp Ni(Al). After 20 hours of milling, additional new peaks were observed, which could all be indexed as a hcp Ni(Al) with the lattice parameters of  $a = 0.2596$  nm and  $c = 0.4390$  nm.

Gradual reduction of NiO was observed as the NiO crystallites were reduced from 60 nm after 5 hours of milling to 40 nm after 20 hours of milling, and 76 pct reduction of NiO was observed after 20 hours of milling (Figure 2). The progress of NiO reduction to 20 hours of milling despite the absence of Al peaks in the XRD pattern indicates the availability of Al in smaller quantity with refined crystallite size or the reduction of NiO carried out by Ni(Al). Less intense peaks of unreacted NiO along with fcc Ni(Al) are also found to exist in 20-hour milled powder. No XRD peaks of  $\text{Al}_2\text{O}_3$  phase were observed in the 20-hour milled powder. This suggests that the  $\text{Al}_2\text{O}_3$  formed as a result of NiO reduction is amorphous in nature and, hence, may not be detected.<sup>[25]</sup> ICP-OES results showed 0.2 wt pct W contamination in 20-hour milled powder.

The DSC traces of 20-hour milled powder presented in Figure 3 show that the transformation of hcp to fcc occurs around 673 K (400 °C). Figure 4 shows the XRD patterns of heat-treated and consolidated 20-hour milled powder. The increase in the fcc Ni(Al) peak intensity and its shift to higher angle side in the 20-hour milled powder heated to 573 K (300 °C) and the presence of only fcc Ni peaks after heating to 773 K (500 °C) indicate that the hcp Ni(Al) has transformed to fcc Ni of  $a = 0.3519$  nm in heating, which could be attributed to grain coarsening. Moreover, the completion of NiO reduction by Al in Ni solid solution also took place in these temperature ranges. XRD pattern of Ni-30 vol pct

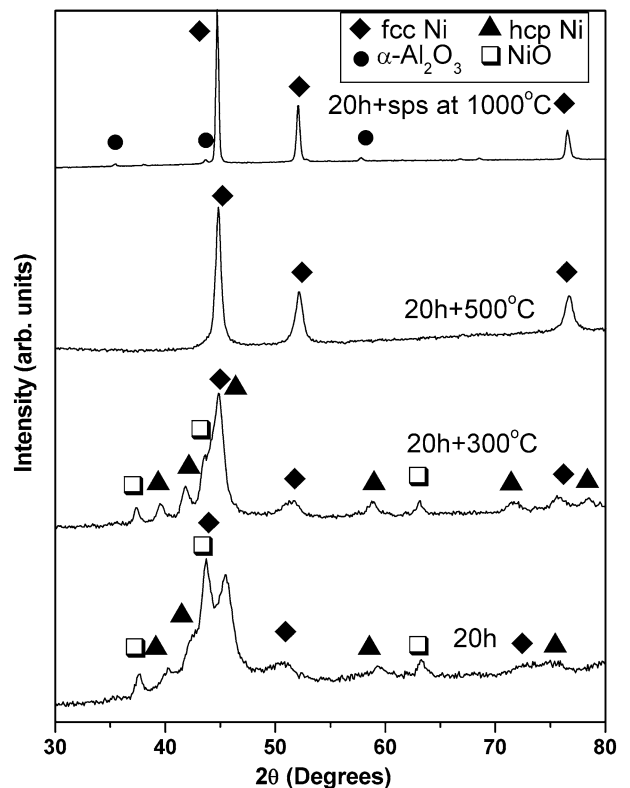


Fig. 4—XRD patterns of NiO, Al, and Ni powder mixture corresponding to Ni-30 vol pct  $\text{Al}_2\text{O}_3$  composition as a function of annealing temperature and after consolidation.

$\text{Al}_2\text{O}_3$  spark plasma sintered at 1273 K (1000 °C) in Figure 4 shows the presence of  $\alpha\text{-Al}_2\text{O}_3$  phase along with the Ni phase. The amorphous  $\text{Al}_2\text{O}_3$  formed in milling transformed to stable  $\alpha\text{-Al}_2\text{O}_3$  on heating. Since the amount of  $\text{Al}_2\text{O}_3$  is small, the heat event associated with the crystallization of  $\alpha\text{-Al}_2\text{O}_3$  is not evident in this DSC trace. However, in the initial study on stoichiometric composition of NiO-Al, which resulted in 60 vol pct  $\text{Al}_2\text{O}_3$  in the product after the completion of reaction, the heat event associated with the crystallization of  $\alpha\text{-Al}_2\text{O}_3$  is clearly seen in the DSC trace.<sup>[26]</sup>

#### B. Microstructural Analysis after SPS Consolidation

For comparison, pure Ni was milled for 20 hours. The crystallite size of Ni after 20 hours of milling is 33 nm. The 20-hour milled pure Ni was then SPS consolidated at 973 K and 1073 K (700 °C and 800 °C). TEM results of bulk Ni samples consolidated at 973 K and 1073 K (700 °C and 800 °C) are shown in Figures 5 and 6, respectively. The bright-field image and the selected area diffraction (SAD) pattern with spotty rings show that the Ni grains are in submicron level. Indexing of the SAD pattern reveals the presence of Ni phase alone. The average grain size of Ni sintered at 973 K (700 °C) is 228 nm (Figure 5(c)) from the dark-field images obtained using Ni(111) and Ni(200) diffraction planes, and for the Ni sample sintered at 1073 K (800 °C), the average grain size is measured to be 375 nm (Figure 6(c)).

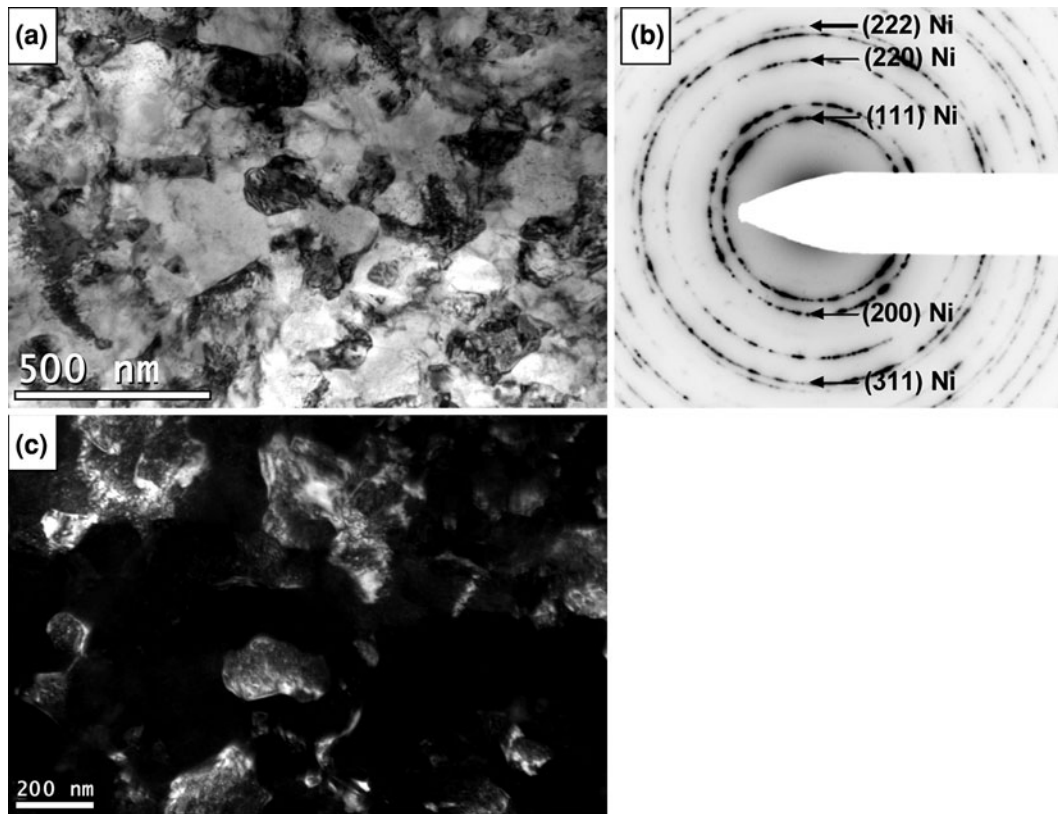


Fig. 5—TEM micrographs of pure Ni sintered at 973 K (700 °C): (a) bright-field image, (b) SAD pattern, and (c) dark-field image obtained from Ni(111) and Ni(200) diffraction rings.

Results of TEM studies on the bulk Ni-30 vol pct  $\text{Al}_2\text{O}_3$  sample SPS at 1273 K (1000 °C) are shown in Figure 7. The SAD pattern in Figure 7(b) shows discontinuous spotty diffraction rings from Ni phase and fine continuous diffraction rings from  $\alpha\text{-Al}_2\text{O}_3$  phase. The average grain size of Ni was measured to be 170 nm from the micrograph. A number of white regions (indicated by the arrow) in the bright-field image in Figure 7(a), were observed in the microstructure. The SAD pattern taken from the white region shows continuous diffraction ring patterns of  $\alpha\text{-Al}_2\text{O}_3$ . The dark-field image (Figure 7(c)) obtained from  $\alpha\text{-Al}_2\text{O}_3$  (012) plane shows the clusters of very fine  $\alpha\text{-Al}_2\text{O}_3$  particles of 6 to 8 nm in the white regions. Around 12 micrographs covering an area of  $200 \mu\text{m}^2$  were taken for calculating the area fraction of the white region consisting of very fine  $\alpha\text{-Al}_2\text{O}_3$  particle clusters. It was found that approximately 0.25 area fraction was occupied by these clusters. The size of the clusters varies from 50 to 1000 nm (Figure 7(d)). Moreover, approximately 0.05 volume fraction of fine  $\alpha\text{-Al}_2\text{O}_3$  particles was also found distributed uniformly in the Ni matrix (Figure 7(e)). Among them, most of the  $\alpha\text{-Al}_2\text{O}_3$  particles are in the 8 to 9 nm size range, while very few of them are in the 20 to 40 nm size range.

### C. Mechanical Properties of Ni and Ni- $\text{Al}_2\text{O}_3$ Nanocomposites

The measured density, grain size, and hardness of the consolidated Ni and Ni-30 vol pct  $\text{Al}_2\text{O}_3$  nanocompos-

ite are listed in Table I. The density of Ni-30 vol pct  $\text{Al}_2\text{O}_3$  nanocomposites after spark plasma consolidation is measured to be 92 pct of theoretical density. The hardness value of Ni-30 vol pct  $\text{Al}_2\text{O}_3$  nanocomposite SPS at 1273 K (1000 °C) was measured to be 4.5 GPa, which is almost 2 times higher than that of monolithic pure Ni SPS at 973 K (700 °C) (2.4 GPa) and 1073 K (800 °C) (2.1 GPa). Compression test results of pure Ni consolidated at 973 K and 1073 K (700 °C and 800 °C) and Ni-30 vol pct  $\text{Al}_2\text{O}_3$  nanocomposites consolidated at 1273 K (1000 °C) are presented in Figure 8. Ni-30 vol pct  $\text{Al}_2\text{O}_3$  nanocomposites exhibit significantly higher strength than the pure Ni sintered at 973 K and 1073 K (700 °C and 800 °C). The loss in ductility, however, seems to be an unfortunate consequence in nanocomposites due to the presence of hard  $\text{Al}_2\text{O}_3$  ceramic particles. The ideal strength deduced from the hardness value is 1380 MPa, which is only 90 MPa higher than the yield strength obtained from the compression test (1290 MPa).

## IV. DISCUSSION

### A. Phase Formation in Ni- $\text{Al}_2\text{O}_3$ Nanocomposites

The fcc Ni(Al) transformed to hcp phase in 15 hours of milling as the fcc Ni(Al) with 9 nm crystallite size and  $6.99 \text{ cm}^3/\text{mol}$  molar volume undergo a defect-induced melting (Lindemann's melting criterion) to amorphous/

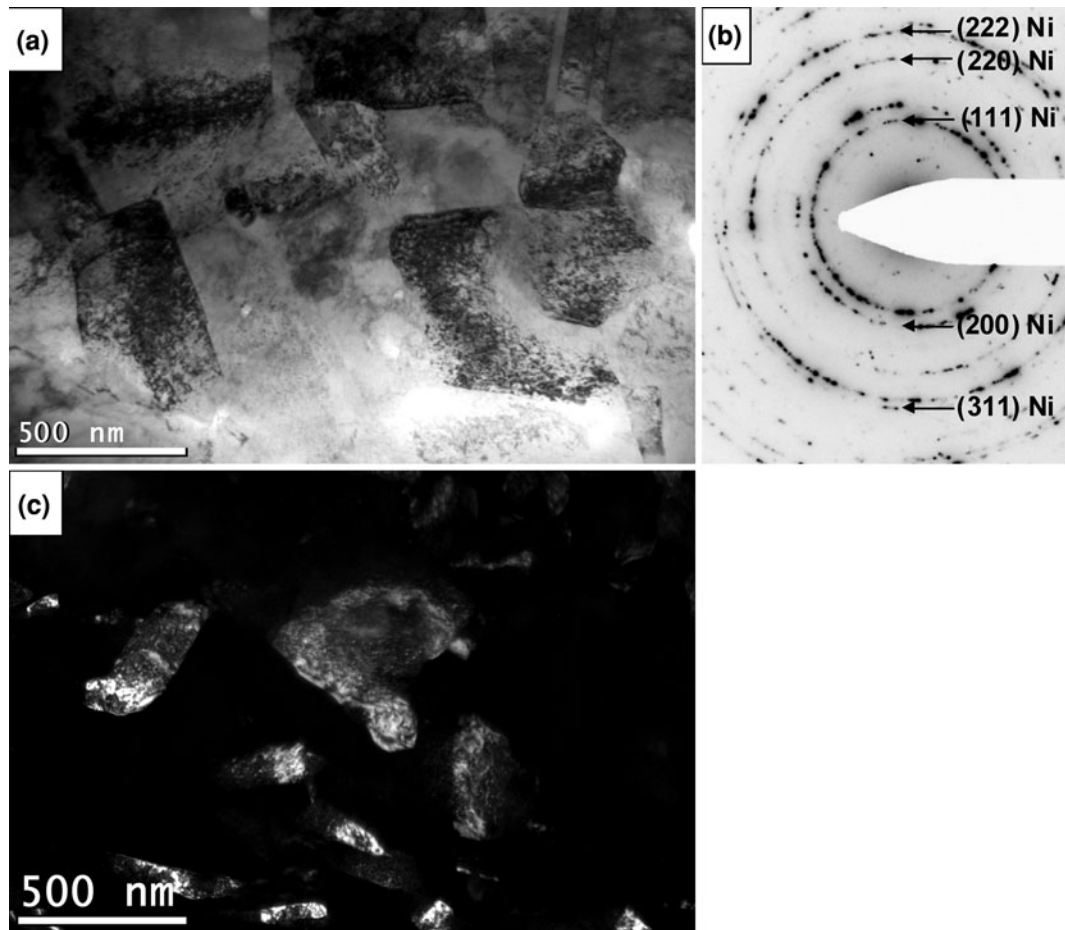


Fig. 6—TEM micrographs of pure Ni sintered at 1073 K (800 °C): (a) bright-field image, (b) SAD pattern, and (c) dark-field image obtained from Ni(111) and Ni(200) diffraction rings.

liquid state that crystallizes into a metastable hcp structure with the molar volume of  $7.7 \text{ cm}^3/\text{mol}$ , which is very close to the molar volume of the liquid at the melting point of Ni ( $7.55 \text{ cm}^3/\text{mol}$ ). The interatomic spacing of nanocrystal increases continuously from core to surface due to lattice softening; hence, the increase in the molar volume of fcc phase with refinement of crystallite size is expected. Datta *et al.*<sup>[27]</sup> reported for the first time the fcc to hcp phase transformation during the mechanical alloying of Ni with Si, when the crystallite size of Ni(Si) reached below 10 nm, which was associated with rapid molar volume increment in fcc Ni(Si). On the other hand, the pure Ni did not show the fcc to hcp transformation during mechanical alloying, since the crystallite size could not be reduced below 20 nm even after 50 hours of milling with the same milling conditions.<sup>[27]</sup> The earlier phase transformation at 15 hours of milling in the present study compared to their study may be due to the presence of hard  $\text{Al}_2\text{O}_3$  particles, which might have increased the crystallite size reduction rate.

### B. Strengthening Mechanisms in Ni- $\text{Al}_2\text{O}_3$ Nanocomposites

Microstructural analysis of Ni-30 vol pct  $\text{Al}_2\text{O}_3$  nanocomposite showed that the grain size is in submi-

cron range and the  $\alpha\text{-Al}_2\text{O}_3$  particles of nanometer size are distributed throughout the matrix. These two features, thus, are expected to contribute significantly to yield strength. In such a condition, yield strength of composite is the result of overall contribution from the matrix, grain size, and particles.

$$\sigma_{0.2} = \sigma_m + \frac{k}{\sqrt{d}} + \sigma_p \quad [1]$$

where  $\sigma_m$  is the strength of the matrix,  $k$  is the Hall–Petch slope,  $d$  is the grain size, and  $\sigma_p$  is the particle strengthening term.

The strengthening contribution from the matrix and grain size can be deduced from the Hall–Petch plot. Figure 9 shows the hardness and grain size data in a Hall–Petch form for the Ni and Ni-30 vol pct  $\text{Al}_2\text{O}_3$  nanocomposites, together with data from several reports for Ni.<sup>[28–32]</sup> Grain size analysis reveals that the grain size of the Ni-30 vol pct  $\text{Al}_2\text{O}_3$  nanocomposites sintered at 1273 K (1000 °C) is slightly smaller (50 nm) than pure Ni sintered at 973 K (700 °C). According to Figure 9, the grain refinement observed in Ni-30 vol pct  $\text{Al}_2\text{O}_3$  nanocomposites can only account for about a 40 MPa increase in strength for this change in grain size. Thus, the additional strengthening of 2.1 GPa in

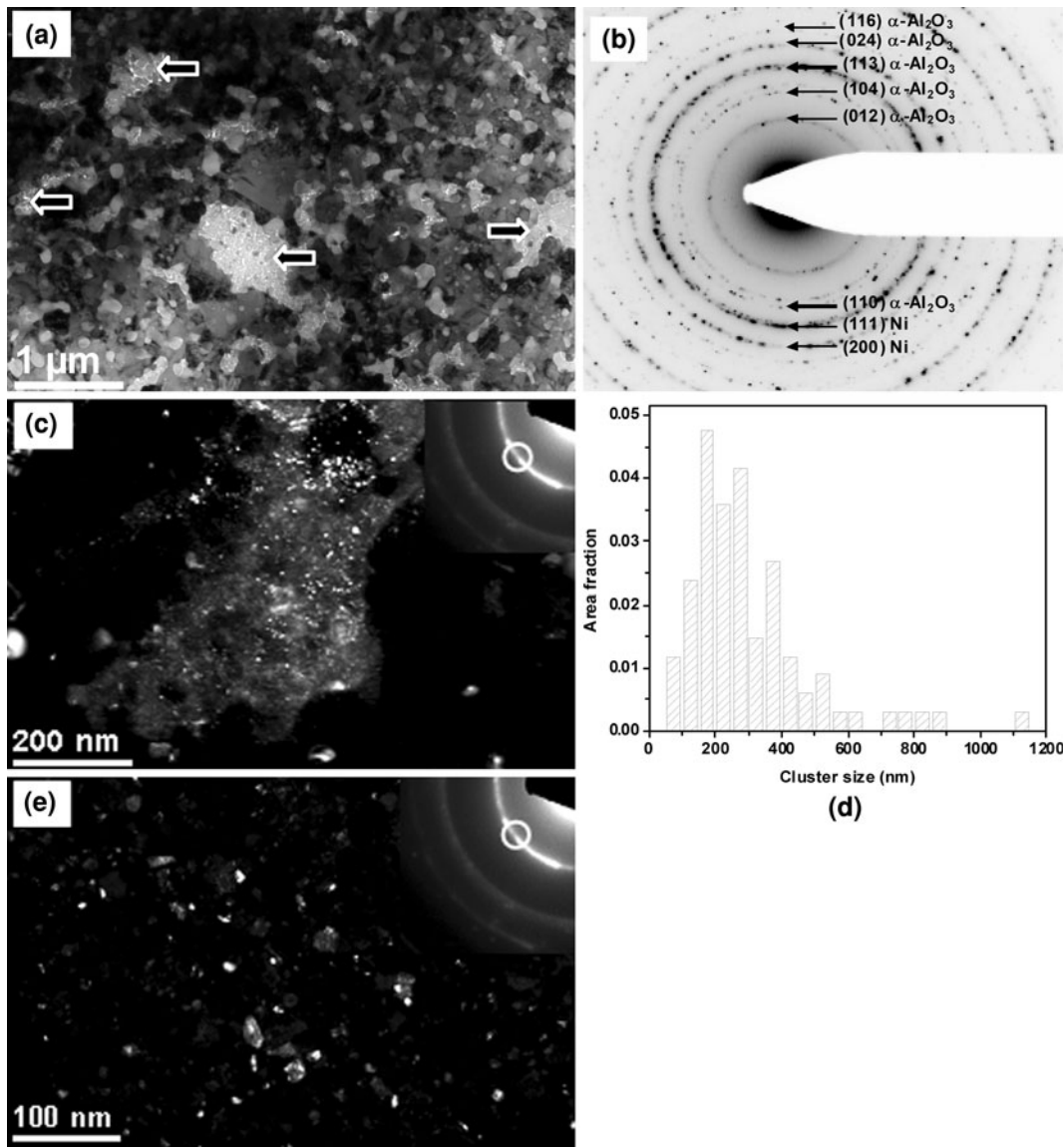


Fig. 7—TEM micrographs of Ni-30 vol pct  $\text{Al}_2\text{O}_3$  nanocomposites: (a) bright-field image, (b) SAD pattern, (c) dark-field image of clusters of fine  $\alpha\text{-Al}_2\text{O}_3$ , (d) size distribution of  $\alpha\text{-Al}_2\text{O}_3$  clusters, and (e) dark-field image of uniformly distributed  $\alpha\text{-Al}_2\text{O}_3$ .

**Table I. Density, Grain Size, and Hardness Values of Consolidated Ni and Ni-30 Vol Pct  $\text{Al}_2\text{O}_3$  Nanocomposites**

Composition	SPS	Density (Pct)	Grain Size (nm)	Hardness $\text{HV}_{0.3}$
	Temperature [K (°C)]			
Ni	973 (700)	94	220	252
	1073 (800)			
Ni-30 vol pct $\text{Al}_2\text{O}_3$	1273 (1000)	92	170	460

Ni-30 vol pct  $\text{Al}_2\text{O}_3$  nanocomposites must be due to the presence of the  $\alpha\text{-Al}_2\text{O}_3$  particles and  $\sim 0.1$  vol pct of WC particles and their interaction with mobile dislocations during plastic deformation. Since the amount of WC particles is much less, the strengthening contribution from  $\text{Al}_2\text{O}_3$  particles alone can be considered.

TEM observation of Ni-30 vol pct  $\text{Al}_2\text{O}_3$  nanocomposite showed that approximately 5 vol pct  $\alpha\text{-Al}_2\text{O}_3$

particles of 8 to 9 nm are distributed uniformly in the Ni matrix. The remaining 25 vol pct of  $\alpha\text{-Al}_2\text{O}_3$  particles are observed in the form of clusters with  $\sim 350$  nm average size. When each cluster is considered as a nondeformable single particle during plastic deformation, Eq. [1] can be rewritten as

$$\sigma_{0.2} = \sigma_m + \frac{k}{\sqrt{d}} + \sigma_{\text{uni}} + \sigma_{\text{cluster}} \quad [2]$$

where  $\sigma_{\text{uni}}$  is the strengthening contribution from uniformly distributed particles and  $\sigma_{\text{cluster}}$  is the strengthening contribution from particle cluster.

Since the uniformly distributed  $\alpha\text{-Al}_2\text{O}_3$  particle size is much smaller than the Ni grain size (170 nm), Orowan-type strengthening will occur in a single grain. Hence, the strengthening contribution for uniformly distributed  $\alpha\text{-Al}_2\text{O}_3$  can be calculated using the following.<sup>[33]</sup>

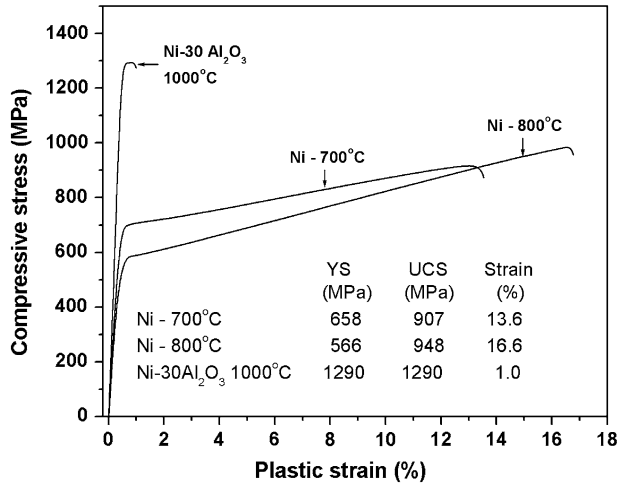


Fig. 8—Compressive stress-strain curves of pure Ni and Ni-30 vol pct Al<sub>2</sub>O<sub>3</sub> nanocomposite.

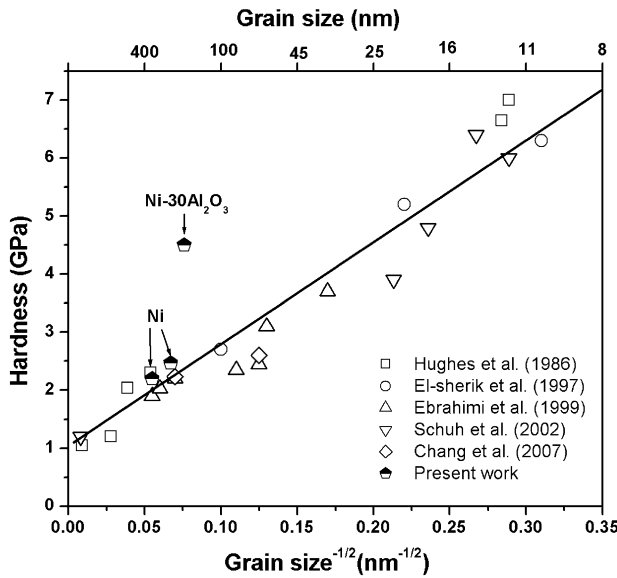


Fig. 9—Hall-Petch plot for pure Ni and Ni-30 vol pct Al<sub>2</sub>O<sub>3</sub> nanocomposite.

$$\sigma_{\text{uni}} = \Delta\sigma_{\text{Oro}} = \frac{2mGb \ln\left\{\frac{\phi}{2b}\right\}}{[(1.18)4\pi(\lambda - \phi)]} \quad [3]$$

where  $\Delta\sigma_{\text{Oro}}$  is the Orowan stress or the stress increase needed to pass a dislocation through an array of impeding particles,  $m$  is the Taylor factor,  $G$  is the shear modulus,  $b$  is the Burgers vector,  $\phi$  is the particle size, and  $\lambda$  is the planar interparticle spacing,  $\phi/\sqrt{V_p}$ , where  $V_p$  is the volume fraction of particle phase.

Since the size of cluster exceeds the grain size of Ni matrix, Orowan-type particle strengthening is not expected. A reasonable approach for analysis in this case can be based on particulate composite strengthening models. The strengthening contribution from particle cluster can be written as<sup>[34]</sup>

$$\sigma_{\text{cluster}} = \sqrt{(\Delta\sigma_{\text{Oro}})^2 + (\Delta\sigma_{\text{load}})^2 + (\Delta\sigma_{\text{the}})^2 + (\Delta\sigma_{\text{geo}})^2} \quad [4]$$

where  $\Delta\sigma_{\text{the}}$  is the strengthening contribution due to statistically stored dislocations introduced by the thermal expansion mismatch between the matrix and particle cluster,  $\Delta\sigma_{\text{geo}}$  is the strengthening contribution due to strain gradient effects associated with the geometrically necessary distributions of dislocations required to accommodate the plastic deformation mismatch between the matrix and the particle cluster, and  $\Delta\sigma_{\text{load}}$  is the strengthening contribution due to load transfer across matrix and particle cluster.

The strengthening contribution due to Orowan stress or stress increase needed to pass a dislocation through an array impeding particle cluster was calculated from Eq. [3].  $\Delta\sigma_{\text{load}}$  is related to the rule-of-mixture effect, and the basic equation is represented by the relationship between the effective composite strength ( $\sigma_{\text{comp}}$ ) and the reference matrix strength ( $\sigma_m$ ):

$$\sigma_{\text{comp}} = V_p\sigma_p + V_m\sigma_m \quad [5]$$

where  $V_m$  is the volume fraction of matrix. The factor  $V_p\sigma_p$ , which is represented by  $\Delta\sigma_{\text{load}}$ , is further expanded using the shear lag model for fibers (this model was later modified to predict the strengthening effect of particles in a matrix). The stress borne by the particle through shear transfer of load at the particle/matrix interface is represented by<sup>[35,36]</sup>

$$\sigma_p = \tau_i s \quad [6]$$

where  $\tau_i$  is the shear stress at the particle matrix interface and  $s$  is the aspect ratio ( $l_p/l_v$ ) of the reinforcing particles, where  $l_p$  and  $l_v$  are the particle size parallel to and vertical to the compressive testing direction, respectively. The particle size is given by  $\phi = \sqrt{l_p l_v}$ . Assuming a well-bonded particle,  $\tau_i$  can be sufficiently accurately represented by  $0.5\sigma_m$  ( $\sigma_m$  is used instead of the yield strength of composite, because it is assumed that the composite yields when the matrix reaches its yield strength). Therefore, particle strength is given by<sup>[37,38]</sup>

$$\sigma_p = 0.5\sigma_m s \quad [7]$$

Substituting Eq. [7] into [5],

$$\sigma_{\text{comp}} = 0.5s\sigma_m V_p + V_m\sigma_m \quad [8]$$

Therefore, the increase in strength due to the presence of particles is given by<sup>[37]</sup>

$$\Delta\sigma_{\text{load}} = 0.5s\sigma_m V_p \quad [9]$$

The strengthening contribution due to thermal expansion mismatch is<sup>[39]</sup>

$$\Delta\sigma_{\text{the}} = \eta Gb\sqrt{\rho} \quad [10]$$

where  $\eta$  is a constant of order 1, and  $\rho$  is the dislocation density. The value of  $\rho$  is given by<sup>[40,41]</sup>

$$\rho = \frac{12\Delta T\Delta\alpha V_p}{bD(1 - V_p)} \quad [11]$$

where  $\Delta\alpha$  is the difference in coefficient of thermal expansion (CTE) between the matrix and the reinforcing particles,  $D$  is the particle size (cluster size is  $\sim 350$  nm), and  $\Delta T$  is the temperature change from processing temperature to room temperature.

Finally, the strengthening contribution due to geometrically necessary dislocations is<sup>[42]</sup>

$$\Delta\sigma_{\text{geo}} = \beta G \sqrt{\frac{V_p \mathbf{b} \varepsilon_m}{D}} \quad [12]$$

where  $\beta$  is a geometric factor with a numerical value  $\sim 0.2$ <sup>[43]</sup> and  $\varepsilon_m$  is the plastic strain of the metal matrix.<sup>[42]</sup>

The parameters required for the theoretical calculation of yield strength of Ni-30 vol pct  $\text{Al}_2\text{O}_3$  nanocomposite are given in Tables II and III. The result of the calculation presented in Figure 10 indicates the influence of thermal mismatch contribution on yield strength of the composite is most significant when the particle is in the form of clusters of 350 nm. Moreover, the theoretical calculation concludes that the Orowan strengthening contribution from clusters  $\Delta\sigma_{\text{Oro}}$  is less significant as the  $\Delta\sigma_{\text{geo}}$  and  $\Delta\sigma_{\text{load}}$ .

The theoretically calculated strengthening contributions from 5 vol pct of uniformly distributed  $\alpha\text{-Al}_2\text{O}_3$  particles and 25 vol pct of particle clusters are 475 and 395 MPa, respectively (Figure 11). The sum of overall strengthening from clusters and the individual  $\alpha\text{-Al}_2\text{O}_3$  particle is 870 MPa. Considering that the corresponding hardness increment is 3 times larger, the hardening due to particles is about 2.6 GPa, which is slightly higher than the experimental results of 2.1 GPa. The possible reason for the difference between theoretically calculated and experimental results might be due to (1) the theoretical calculation was made assuming that all the particles are within the grains. However, a significant amount of particles may be present in the grain boundary, which is less important for the thermal stress

**Table II. Parameters Used in Theoretical Calculation of Yield Strength in Ni-30 Vol Pct  $\text{Al}_2\text{O}_3$  Nanocomposites**

Parameter, Unit	Value	Reference
$m$	3	23
$G$ , GPa	76	23
$\mathbf{b}$ , nm	0.249	23
CTE of Ni, $^{\circ}\text{C}^{-1}$	$13.2 \times 10^{-6}$	44
CTE of $\text{Al}_2\text{O}_3$ , $^{\circ}\text{C}^{-1}$	$9 \times 10^{-6}$	45
$\varepsilon_m$	0.1	46

**Table III. Experimentally Obtained Parameters Used in Theoretical Calculation of Yield Strength in Ni-30 Vol Pct  $\text{Al}_2\text{O}_3$  Nanocomposites**

System	Sintering Temperature [K ( $^{\circ}\text{C}$ )]	Uniformly Distributed $\alpha\text{-Al}_2\text{O}_3$		Clusters of $\alpha\text{-Al}_2\text{O}_3$	
		Size (nm)	Volume Fraction	Size (nm)	Volume Fraction
Ni-30 vol pct $\text{Al}_2\text{O}_3$	1273 (1000)	8	0.05	350	0.25

and dislocation. (2) The error in calculating the volume fraction of cluster from TEM analysis and the volume fraction of cluster measurement may not be very accurate, and a small error in measure will lead to significant change in the theoretically calculated hardness value. For example, if the measured volume fraction of clusters is 0.26 instead of 0.25, the calculated hardness value will decrease from 2.6 to 2.3 GPa. The results of theoretically calculated strengthening contributions from uniformly distributed and clusters of particles in Ni-30 vol pct  $\text{Al}_2\text{O}_3$  nanocomposite

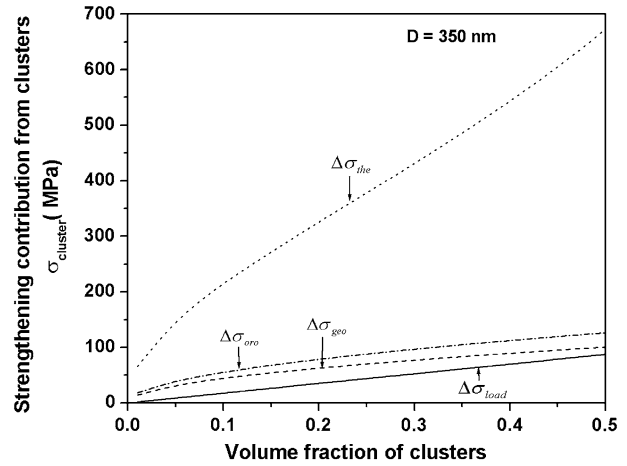


Fig. 10—Theoretically calculated strengthening contribution from  $\alpha\text{-Al}_2\text{O}_3$  clusters in Ni-30 vol pct  $\text{Al}_2\text{O}_3$  nanocomposite.

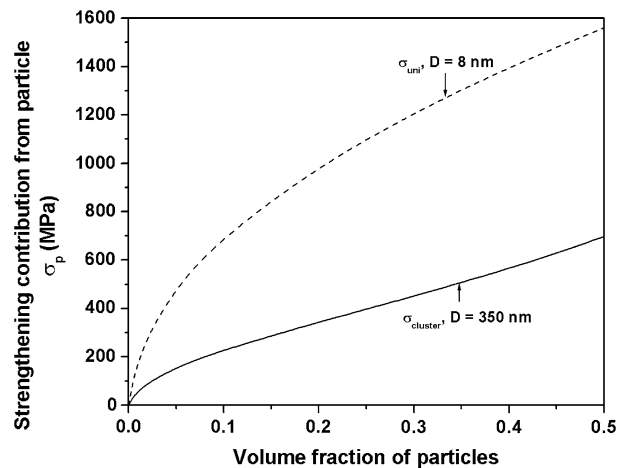


Fig. 11—Comparison of theoretically calculated strengthening contribution from uniformly distributed and clusters of  $\alpha\text{-Al}_2\text{O}_3$  particles in Ni-30 vol pct  $\text{Al}_2\text{O}_3$  nanocomposite.



presented in Figure 11 also show that for the same volume fraction, strengthening contribution from uniformly distributed particles of 8 nm is 3 times higher than that of the particle cluster of 350 nm. Hence, the real potential of the synthesized composite can be achieved if the clusters are broken into individual particles and distributed uniformly in the matrix.

The loss in ductility, however, seems to be an unfortunate consequence of the grain boundary pinning mechanism. Particles present at the pinned grain boundaries act as nucleation sites for deformation-induced grain boundary cavities.<sup>[47]</sup> This increased tendency for grain boundary cavitation may lead to a decrease in overall ductility in these particulate composite materials.<sup>[47–50]</sup> Microstructure revealed that agglomerations of reinforcement particles caused local stress concentrations in the composite and led to crack formation in the matrix. Presence of hard and brittle Al<sub>2</sub>O<sub>3</sub> particles in the ductile Ni matrix exerts constraints on the plastic flow of the matrix. When combined with concentration and triaxiality of stress in clustered particle regions, the composite undergoes brittle fracture without showing appreciable ductility.<sup>[51]</sup>

## V. CONCLUSIONS

Bulk Ni-30 vol pct Al<sub>2</sub>O<sub>3</sub> *in-situ* nanocomposite was developed successfully by carrying out reactive milling for NiO-Al-Ni powder mixture and subjecting the as-milled powder to SPS at 1273 K (1000 °C). Gradual NiO reduction and simultaneous Ni(Al) formation were observed during milling. Interestingly, fcc to hcp transformation was also observed in Ni(Al) phase during milling, and it completely transformed back to fcc phase around 773 K (500 °C) in heating. The measured hardness and the yield strength of synthesized Ni-30 vol pct Al<sub>2</sub>O<sub>3</sub> nanocomposite (4.5 GPa and 1290 MPa, respectively) is 2 times higher than that of pure Ni of similar grain size, which is mainly attributed to the presence of alumina particles of nanometer size.

## REFERENCES

1. S.C. Tjong and Z.Y. Ma: *Mater. Sci. Eng.*, 2000, vol. 29R, pp. 49–113.
2. B.S. Murty and S. Ranganathan: *Int. Mater. Rev.*, 1998, vol. 43, pp. 101–41.
3. C. Suryanarayana: *Prog. Mater. Sci.*, 2001, vol. 46, pp. 1–184.
4. P.K. Sinha, N. Dhananjayan, and H.K. Chakrabarti: *Plating*, 1973, vol. 60, pp. 55–59.
5. B. Muller and H. Ferkel: *Mater. Sci. Forum*, 2000, vols. 343–346, pp. 476–81.
6. M.E. Bahrololoom and R. Sani: *Surf. Coat. Technol.*, 2005, vol. 192, pp. 154–63.
7. A. Jung, H. Natter, R. Hempelmann, and E. Lach: *J. Mater. Sci.*, 2009, vol. 44, pp. 2725–35.
8. S.T. Aruna, C.N. Bindu, V.E. Selvi, V.K.W. Grips, and K.S. Rajam: *Surf. Coat. Technol.*, 2006, vol. 200, pp. 6871–80.
9. L. Benea: *Mater. Manuf. Processes*, 1999, vol. 14, pp. 231–42.
10. P.A. Gay, P. Bercot, and J. Pagetti: *Surf. Coat. Technol.*, 2001, vol. 140, pp. 147–54.
11. A. Moller and H. Hahn: *Nanostruct. Mater.*, 1999, vol. 12, pp. 259–62.
12. M.N. Joshi and M. Totalani: *J. Electrochem. Soc. India*, 1979, vol. 28, pp. 35–40.
13. G.N.K.R. Babu, V.S. Muralidharan, and K.I. Vasu: *Plat. Surf. Finish.*, 1991, vol. 78, pp. 126–33.
14. V. Medeliene, R. Juskenas, and M. Kurtinaitiene: *Pol. J. Chem.*, 2004, vol. 78, pp. 1305–17.
15. M. Kaisheva and J. Fransaer: *J. Electrochem. Soc.*, 2004, vol. 151C, pp. 89–96.
16. K.M. Ibrahim, A.A. Aal, and Z.A. Hamid: *Int. J. Cast Met. Res.*, 2005, vol. 18, pp. 315–20.
17. F. Hu and K.C. Chan: *Appl. Surf. Sci.*, 2004, vol. 233, pp. 163–71.
18. M. Surender, R. Balasubramaniam, and B. Basu: *Surf. Coat. Technol.*, 2004, vol. 187, pp. 93–97.
19. M. Stroumbouli, P. Gyftou, and E.A. Pavlatou: *Surf. Coat. Technol.*, 2005, vol. 195, pp. 325–32.
20. M. Surender, B. Basu, and R. Balasubramaniam: *Proc. Int. Conf on Advances in Surface Treatment: Research & Applications (AS-TRA)*, ASM international, Metal Park, OH, 2004, pp. 130–34.
21. J.L. Endrino, J.J. Nainaparampil, and J.E. Krzanowski: *Surf. Coat. Technol.*, 2002, vol. 157, pp. 95–101.
22. S. Eroglu and B. Gallois: *J. Mater. Sci.*, 1995, vol. 30, pp. 1754–59.
23. S.H. Goods, T.E. Buchheit, R.P. Janek, J.R. Michael, and P.G. Kotula: *Metall. Mater. Trans. A*, 2004, vol. 35A, pp. 2351–60.
24. T.H. De Keijser, J.I. Langford, E.J. Mittemeijer, and A.B.P. Vogel: *J. Appl. Cryst.*, 1982, vol. 15, pp. 308–14.
25. V. Udhayabanu, K.R. Ravi, V. Vinod, and B.S. Murty: *Intermetallics*, 2010, vol. 18, pp. 353–58.
26. V. Udhayabanu, Navneet Singh, and B.S. Murty: *J. Alloys Compd.*, 2010, vol. 497, pp. 142–46.
27. M.K. Datta, S.K. Pabi, and B.S. Murty: *J. Mater. Res.*, 2000, vol. 15, pp. 1429–32.
28. G.D. Hughes, S.D. Smith, C.S. Pande, H.R. Johnson, and R.W. Armstrong: *Scripta Mater.*, 1986, vol. 20, pp. 93–97.
29. A.M. El-Sherik, U. Erb, G. Palumbo, and K.T. Aust: *Scripta Mater.*, 1997, vol. 22, pp. 1185–88.
30. F. Ebrahimi, G.R. Bourne, M.S. Kelly, and T.E. Matthews: *Nanostruct. Mater.*, 1999, vol. 11, pp. 343–50.
31. C.A. Schuh, T.G. Nieh, and T. Yamasaki: *Scripta Mater.*, 2002, vol. 46, pp. 735–40.
32. L. Chang, P.W. Kao, and C.H. Chen: *Scripta Mater.*, 2007, vol. 56, pp. 713–16.
33. D.G. Morris, I. Gutierrez-Urrutia, and M.A. Munoz-Morris: *Scripta Mater.*, 2007, vol. 57, pp. 369–72.
34. F.J. Humphreys, S.I. Anderson, H. Lilholt, and O.B. Pedersen: *9th Riso Int. Symp. on Metallurgy and Materials Science*, Riso National Laboratory, Roskilde, Denmark, 1988, pp. 51–74.
35. V.C. Nardone and K.M. Prewo: *Scripta Metall.*, 1986, vol. 20, pp. 43–48.
36. M.R. Piggot: *Load Bearing Fibre Composites*, Pergamon Press, Oxford, United Kingdom, 1980.
37. N. Ramakrishnan: *Acta Metall.*, 1996, vol. 44, pp. 69–77.
38. H.W. Zhang, R. Gopalan, T. Mukai, and K. Hono: *Scripta Mater.*, 2005, vol. 53, pp. 863–68.
39. N. Hansen: *Acta Metall.*, 1977, vol. 25, pp. 863–68.
40. R.J. Arsenault, L. Wang, and C.R. Feng: *Acta Metall. Mater.*, 1991, vol. 39, pp. 47–57.
41. R.J. Arsenault and N. Shi: *Mater. Sci. Eng.*, 1986, vol. 81, pp. 175–87.
42. L.M. Brown and W.M. Stobbs: *Phil. Mag.*, 1976, vol. 34, pp. 351–72.
43. T.W. Clyne and P.J. Withers: *An Introduction to Metal Matrix Composites*, Cambridge University Press, New York, NY, 1993.
44. K.H. Zuo, D.L. Jiang, and Q.L. Lin: *Mater. Lett.*, 2006, vol. 60, pp. 1265–68.
45. S. Schicker, D.E. Garcia, J. Bruhn, R. Janssen, and N. Claussen: *J. Am. Ceram. Soc.*, 1997, vol. 80, pp. 2294–300.
46. M.A. Munoz-Morris, C. Garcia Oca, and D.G. Morris: *Acta Mater.*, 2002, vol. 50, pp. 2825–36.
47. S.H. Goods and L.M. Brown: *Acta Metall.*, 1979, vol. 27, pp. 1–15.
48. S.H. Goods and W.D. Nix: *Acta Metall.*, 1978, vol. 26, pp. 739–52.
49. R. Raj: *Flow and Fracture at Elevated Temperatures*, ASM, Metals Park, OH, 1985.
50. H. Reidel: *Fracture at High Temperatures*, Springer-Verlag, New York, NY, 1986.
51. S. Yotte, D. Breyse, J. Riss, and S. Ghosh: *Mater. Characterization*, 2001, vol. 46, pp. 211–19.